Influence of nucleosome structure on the three-dimensional folding of idealized minichromosomes

Jennifer A Martino, Vsevolod Katritch and Wilma K Olson*

Background: The closed circular, multinucleosome-bound DNA comprising a minichromosome provides one of the best known examples of chromatin organization beyond the wrapping of the double helix around the core of histone proteins. This higher level of chain folding is governed by the topology of the constituent nucleosomes and the spatial disposition of the intervening protein-free DNA linkers.

Results: By simplifying the protein–DNA assembly to an alternating sequence of virtual bonds, the organization of a string of nucleosomes on the minichromosome can be treated by analogy to conventional chemical depictions of macromolecular folding in terms of the bond lengths, valence angles, and torsions of the chain. If the nucleosomes are evenly spaced and the linkers are sufficiently short, regular minichromosome structures can be identified from analytical expressions that relate the lengths and angles formed by the virtual bonds spanning the nucleosome-linker repeating units to the pitch and radius of the organized quaternary structures that they produce.

Conclusions: The resulting models with 4–24 bound nucleosomes illustrate how a minichromosome can adopt the low-writhe folding motifs deduced from biochemical studies, and account for published images of the 30 nm chromatin fiber and the simian virus 40 (SV40) nucleohistone core. The marked sensitivity of global folding to the degree of protein–DNA interactions and the assumed nucleosomal shape suggest potential mechanisms for chromosome rearrangements upon histone modification.

Addresses: Department of Chemistry, Rutgers, The State University of New Jersey, Wright-Rieman Laboratories, 610 Taylor Road, Piscataway, NJ 08854-8087, USA.

*Corresponding author.
E-mail: olson@rutchem.rutgers.edu

Key words: computer models, DNA higher-order structure, minichromosomes, nucleosome-induced folding

Received: 15 February 1999
Revisions requested: 29 March 1999
Revisions received: 29 April 1999
Accepted: 4 May 1999

Published: 28 July 1999

Structure August 1999, 7:1009–1022
http://biomednet.com/elecref/0969212600701009

 ISSN 0969-2126

Introduction

The inherent utility of the structural attributes of proteins and nucleic acids in supporting and catalyzing life-sustaining processes is substantiated with each novel crystal form unveiled. Thus far, limited by molecular size and flexibility, the form–function relationships have focused on protein tertiary structure [1,2] and variations in the DNA double helix at the base-pair level [3]. However, there is increasing evidence that DNA tertiary structure may play a role in supporting genetic regulation. Early suspicions born of visualizations of critical transcription enzymes and associated factors redirecting the path of the DNA duplex upon complex formation [4–6] have been substantiated by biochemical studies of intrinsically curved sequences that mimic the genetic function of these proteins [7]. In addition, long-range chain folding by proteins previously known only to provide packaging services have been shown, in isolated cases, to bring remotely bound factors into close contact, indirectly catalyzing genetic activity [8]. This level of global DNA tertiary structure, which has traditionally eluded detailed visualization, is conveniently represented through computer modeling.

The present study focuses on the configurational effects of a naturally abundant protein–DNA complex, the nucleosome, on the path of the chromatin fiber. Nucleosomes, which provide the first level of packaging of the genetic code into the nucleus, distort the local trajectory of the double helix more than nearly any other protein complex examined to date. The tight wrapping of DNA about the core of eight histone proteins — 146 residues wrapped 1.65 left-handed superhelical turns about the 85–90 Å diameter protein assembly [9] — bends the DNA as much as 30° per base pair and an average of ~3° per dimer step. Here, we investigate the next level of chromatin organization, radial chromosome loops [10], by modeling multinucleosomal DNA rings, or minichromosomes [11–13], which approximate the biologically relevant structures. We develop analytical expressions to identify the configurations of histone-bound polymers directly, taking advantage of the simple representation of nucleosome-bound DNA commonly used to interpret low-resolution (cryo-electron and scanning-force) microscopic images of chromatin fibers [14–17], namely, a regular alternating sequence of protein-bound superhelices and straight DNA linkers of constant length (see Figure 1). The assumed

Figure 1

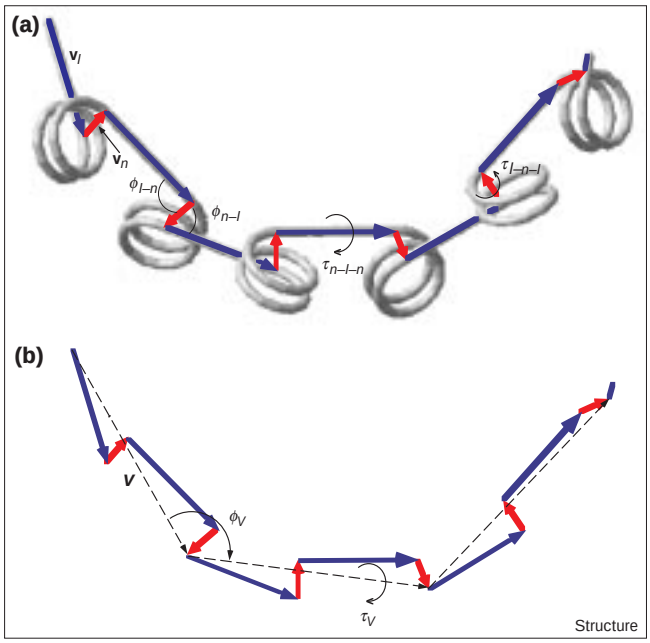

Path of the DNA double helical axis in two minichromosome fragments illustrating local geometric and extended virtual bond parameters of the closed chain. Long (blue) and short (red) vectors in **(a)** represent linker v_l and nucleosomal v_n segments, respectively, and define the pseudo bond lengths (v_l, v_n), valence angles (ϕ_{l-n}, ϕ_{n-l}), and torsion angles (τ_{l-n-l}, τ_{n-l-n}) used to mimic the presence of protein cores on the DNA. Dashed vectors in **(b)** illustrate the assumed dinucleosomal repeating elements and the extended virtual bonds (V), virtual angles (ϕ_V), and virtual torsions (τ_V) used to identify closed circular chains.

even spacing of nucleosomes mimics a structural regularity well known in the organization of DNA in the 30 nm fiber [18–21], whereas the stiff linkers approximate the preferred spatial configuration of short, random sequence B-DNA [3]. Other independent parameters of the model include the length of linker DNA and the style and degree of superhelical wrapping.

The introduction of linear segments in the protein-free linkers automatically yields chromatin models of zero bending energy. If the interactions of protein-bound DNA are omitted from the calculations, the energetic differences among possible chain configurations simply arise in the long-range nonbonded contributions and in the twisting of linker segments. We further assume that linker segments are nicked, so that the twisting energy is zero. Because state of the art computer simulations have not yet advanced to the point where it is possible to estimate the magnitudes of protein–DNA interactions routinely [22], we assume a fixed energy term for all nucleosomes on a given molecule, and in the absence of reliable quantitative estimates of the inter-nucleosomal forces that are thought to govern chromatin structure [23], we consider all sterically acceptable closed circular DNA configurations. Despite this crude energetic treatment, the requirements on chain closure place stringent limitations on the numbers of nucleosomes, the specific styles of protein wrapping, and the global folding of our minichromosome models.

Two sets of minichromosome chains are considered. In the first set, the amount of DNA bound to each phantom histone octamer is varied. The repeat length (nucleosomal plus linker DNA) is fixed at 207 base pairs (bp) per chromatosome, a popular size in experimental work [13], and the DNA path is taken to be a regular left-handed superhelix of 45 Å radius and 30 Å pitch. A follow-up investigation includes the same nucleosome wrapping style, but relaxes the repeat length to search for closed chain configurations with 20–100 bp linker segments. The phantom protein core is deformed in the second set of minichromosome models over a wide range of barrel or capstan shapes. The amount of bound DNA is fixed at 146 bp and the nucleosome-linker repeat length at 207 bp, while the pitch of wrapping is reduced to 27 Å. This change of shape is consistent with evidence supporting non-cylindrical nucleosome particles [24–26] and well-accepted proposals suggesting that the histone core may undergo a subtle change in shape with post-translational histone modifications, such as acetylation or phosphorylation [27–30]. The number of nucleosomes per DNA ring ranges from 4 to 24, yielding minichromosome models of 828–4968 bp. Thus, the largest model closely matches the naturally occurring SV40 minichromosome in terms of number of bound proteins and total contour length [11]. The variety of encountered structures provides new insights into a wide array of biologically relevant DNA topics, including linking number changes in minichromosomes, nucleosomes as agents of genetic control, and folding of DNA in chromatin.

Results

DNA rings bound by cylindrical histone octamers on 207 bp repeat lengths

A sampling of global equilibrium configurations of minichromosomes with even numbers of bound nucleosomes is presented, in stereo, in Figure 2. The nucleosomes in these structures wrap 1.5–1.9 left-handed superhelical turns of DNA at a pitch of 30 Å/turn, around cylinder-shaped phantom histone cores of 45 Å radius. The amount of DNA bound per protein constraint is a constant for all nucleosomes in a given structure and the linker length is adjusted so that the nucleosome–linker units contain 207 bp. Pertinent data on these and other closed circular chains, generated at 1° increments of the linker torsion τ_{n-l-n} in a dinucleosomal virtual repeating unit (see the Materials and methods section), are organized in Table 1.

The most obvious feature of the minichromosome models in Figure 2 is their highly variable three-dimensional nature. The different degrees of protein–DNA interaction

Figure 2

Stereoviews of the global equilibrium configurations of four minichromosome models binding phantom histone octamers with (a) 1.5, (b) 1.6, (c) 1.7, and (d) 1.9 superhelical turns of DNA. Bound DNA is evenly spaced on nucleosome–linker repeats of 207 bp in all cases. Chains in (a–c) bind 12 cylinder-shaped octamers with 45 Å radii and 30 Å pitch, whereas the ring in (d) binds 14 such octamers.

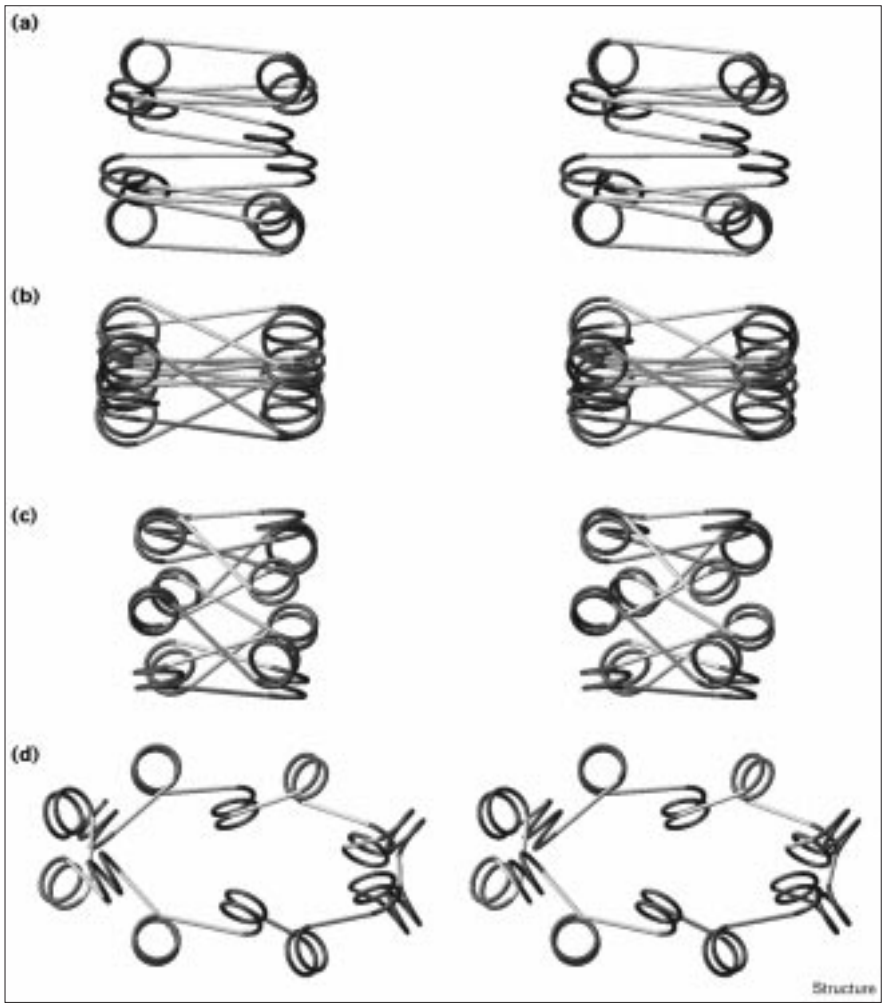

define distinct folding motifs that are common to all chains with a given degree of wrapping. For example, the organization of minichromosomes with 1.5 turns of bound DNA per nucleosome is reminiscent of a cooling coil in an air-conditioning unit, except for the circularization of the overall spatial pathway (see Figure 2a). The global radii of such structures increase with the number of bound nucleosomes (see values of the global radius ρ in Table 1). The additional wrapping of DNA in the 1.6-turn structural family folds the minichromosome into a tightly packed bundle with many inter-linker contacts at the center of the assembly (see Figure 2b). This global structure is relatively narrow, giving the appearance of a sheaf of wheat, and the radius is relatively insensitive to the number nucleosomes. The minimum energy structures with 1.7 or 1.75 superhelical turns of bound DNA, by contrast, resemble bottomless woven baskets, especially when the number of nucleosomes per minichromosome exceeds six and the central opening is fairly large (see Figure 2c). Here, alternate sequential nucleosomes lie on opposite rims of the 'basket', and the global radius gradually increases with the number of protein-bound units. If DNA wrapping is further increased to 1.85–1.95 turns, the minichromosome chains become less globular, forming nearly planar polygons, while maintaining a criss-cross pattern in the linker DNA as it enters and exits each fixed supercoil (see Figure 2d).

As is evident from Table 1, only selected levels of protein–DNA interaction yield closed chains with under 25 evenly spaced nucleosomes. There are no examples in the table of circular chains with protein-bound fragments of 1.55, 1.65, 1.8 or 2.0 superhelical turns on 207 bp nucleosome–linker segments. In addition, different degrees of DNA–protein association produce closed structures in different size regimes; for example, the DNA segments entering and exiting nucleosomes of 1.5 superhelical turns are roughly parallel. Thus, closed chains with nearly any number of such nucleosomes can form. By contrast, the DNA emerging from 1.85–1.95 turns of superhelical

Table 1

Global equilibrium configurations of nicked DNA rings bound by cylindrical histone octamers on 207 bp repeat lengths.

T	L_{link} (bp)	$\tau_{n_1-l_1-n_2}$ (deg)	$\tau_{n_2-l_2-n_1}$ (deg)	N_{core}	ρ (Å)	Wr
1.5	82	167	–12	4	114	–5.0
		–141	–20	6	136	–7.7
		–91	–31	12	202	–16.2
		–85	–33	14	222	–18.6
		–80	–35	16	246	–20.2
		–72	–39	22	314	–29.4
1.55	–	–	–	–	–	–
1.6	73	93	–91	4	106	–6.3
		92	–30	6	107	–9.6
		91	–1	8	109	–13.4
		91	17	10	110	–16.3
		91	29	12	113	–19.9
1.65	–	–	–	–	–	–
1.7	65	139	–82	4	133	–6.4
		124	–23	6	143	–9.9
		11	21	10	172	–17.5
		106	32	12	190	–21.3
1.75	61	160	–119	4	137	–6.6
		127	–44	6	160	–10.1
		114	–14	8	182	–13.9
		106	4	10	206	–17.6
1.8	–	–	–	–	–	–
1.85	52	119	–93	8	213	–13.8
		100	–64	10	251	–17.6
1.9	48	93	–84	14	347	–24.7
1.95	46	103	–108	24	589	–42.6
2.0	–	–	–	–	–	–

Independent variables of idealized minichromosome models: T, the number of superhelical turns of DNA in the geometrically fixed protein-bound coils; L_{link}, the contour length of linker DNA; $\tau_{n_1-l_1-n_2}$ and $\tau_{n_2-l_2-n_1}$, the variable torsion angles in the chain backbone, where the subscripts distinguish nucleosomes and linkers in the assumed 'dimeric' conformational repeat. Dependent parameters: N_{core}, the number of bound nucleosomes: ρ, the global radius of DNA at the nucleosome–linker junction; Wr, the writhing number of the closed ring. The contour length of nucleosomal DNA, L_{core}, can be obtained from T, the assumed radius (R = 45 Å), and the superhelical pitch (P = 30 Å):

$$L_{core} = T\sqrt{P^2 + (2\pi R)^2}$$

See text for further details.

wrapping is pointed in opposite directions, defining a wide DNA exit/entry angle. Formation of a closed minichromosome accordingly requires a large number of repeating units. It is also plain from Table 1 that the writhing number, Wr, the measure of the global folding of a minichromosome chain used here, increases with chain complexity, that is, with both the number of protein-bound segments of a given type and the degree of wrapping around protein cores.

The different families of minichromosome structures further orient the constituent supercoiled and linear fragments in unique spatial patterns. For example, 1.6-turn protein complexes that are remote along the DNA contour remain spatially close, regardless of the number of constituent nucleosomes. This is the only family of closed structures with intimate contacts between distant linkers in chains of all sizes. While close contacts of the negatively charged sugar-phosphate backbone are typically associated with structural instability, the proximity of distant linker fragments provides an opportunity for remotely bound transcription factors to interact or for recombination events to proceed. The slight decrease in superhelical wrapping in the 1.5-turn family of minichromosome structures leads to a completely different pattern of nonbonded interactions. The roughly parallel alignment of alternating nucleosomes in these structures enhances interactions between histone cores. The close contacts of protein-bound DNA, which are less than the linker length, are relevant to higher-order chromatin packaging models [14,19–21] and the condensed forms of chromatin observed at high salt [31].

Quantitative analysis of the chains reported in Table 1 reveals several structural insights, including a relatively large variation in the writhe per nucleosome, that is, $Wr \div N_{core}$ from Table 1, among chains with a given degree of superhelical wrapping. The spread in nucleosomal writhe with the addition of bound protein segments is greatest in the 1.7-turn family of structures. The writhing contribution per nucleosome decreases from –1.6 in the four-nucleosome circle to –1.8 in the example with 12 nucleosomes. By contrast, there is no simple dependence of Wr per protein core on the number of bound nucleosomes in other families of closed structures. The drop in writhe per nucleosome associated with an increase in superhelical wrapping is consistent with previous investigations of protein-bound, circular DNA [32–34]. The ~0.3 decrease in core writhe brought about by the uptake (from 1.5 to 1.6 turns) of DNA onto the histone octamer corresponds closely with the folding change associated with the elastic transition of a mononucleosomal chain subject to the identical increment in superhelical wrapping [34,35]. The changes in Wr seen here in multinucleosomal rings, however, are smaller than values reported previously for similar events in DNA chains with a single set of histone proteins [33,34]. As pointed out elsewhere [35,36], Wr is a global property and not an additive quantity, obtained by assigning a unit value per bound protein. Therefore, as system conditions change in terms of the number of bound proteins, degree of superhelical wrapping per core etc., the writhe per nucleosome and its contribution to the change in ΔLk upon ligation of nicked chains (see below) also change.

Extension of the current study to circular chains with different linker lengths confirms the preceding conformational picture. The writhing numbers of the minichromosome models are stable against changes in linker length from 20 to 100 bp (see Figure 3). These limits encompass the range of linkers witnessed in naturally

occurring DNA [37] and avoid the steric clash of sequential nucleosomes [38]. Longer DNA linkers are not expected to follow the linear course assumed here, given that the persistence length of DNA is ~150 bp [39]. The writhing numbers of such chains will be influenced by room temperature fluctuations of individual base pairs [40], even if the straight path has the lowest bending energy. Finally, changes in linker length within the 20–100 bp range have no effect on the variation in *Wr* brought about by increasing numbers of bound nucleosomes (Figure 3).

DNA rings binding capstan-shaped nucleosomes on 207 bp repeat lengths

The second set of models incorporates a more precise description of nucleosomal DNA. The amount of DNA wrapped about the phantom protein core is fixed at 146 bp, a value that has been obtained repeatedly in nucleosome-digestion experiments [41–43], while the pitch of bound (left-handed superhelical) DNA is set at 27 Å per turn, for improved consistency with experimentally determined values [9]. The pitch is a critical parameter in our models as it helps to set the angle at which free DNA emerges from the complex. Here, the nucleosomes are subjected to a series of distortions that address the diversity of shapes proposed for the core particle under various experimental conditions [24–26] and anticipated at various stages of the cell cycle [27–30]. The phantom protein cylinder is smoothly deformed to a capstan shape by flaring the ends of the cylinder, equally, to radii exceeding 45 Å, while fixing the radius at the dyad, R_0, at 45 Å. Such modifications not only mimic the kind of bulging of the core particle witnessed under low-salt conditions [44] but also help to account for the change of linking number tied to nucleosome formation [45]. This series of configurations sheds light on the dynamic nature of the core particle structure proposed in connection with histones H2A and H2B and with linker histone variant molecules that are encountered during organism development [29] and through chemical modification, such as acetylation or phosphorylation [27,28,30].

Systematic adjustment of the shape of the core particle changes the superhelical wrapping of the fixed number of bound base pairs. As the outer radius, R_e, increases from 45 to 65.7 Å, the number of superhelical turns concomitantly decreases from 1.75 in the ideal cylinder to 1.5 in the most severely distorted shapes. Given that the degree of superhelical wrapping remains a topic of debate [15,46,47], modeling these different forms is reasonable. The linker length is fixed at 61 bp in all cases so that the nucleosomes are evenly spaced on 207 bp repeats. Pertinent data are summarized in Table 2.

Like the cylinder-shaped nucleosomes, the capstan-shaped cores readily form closed DNA chains bearing protein-bound segments. The deformed complexes adopt global structures closely resembling those found for DNA wrapping the corresponding number of turns around cylindrical protein cores. For example, minichromosomes with ends flared to 65.7 Å, where $R_e/R_0 = 1.46$, organize in multinucleosomal rings much like those reported in Figure 2a

Figure 3

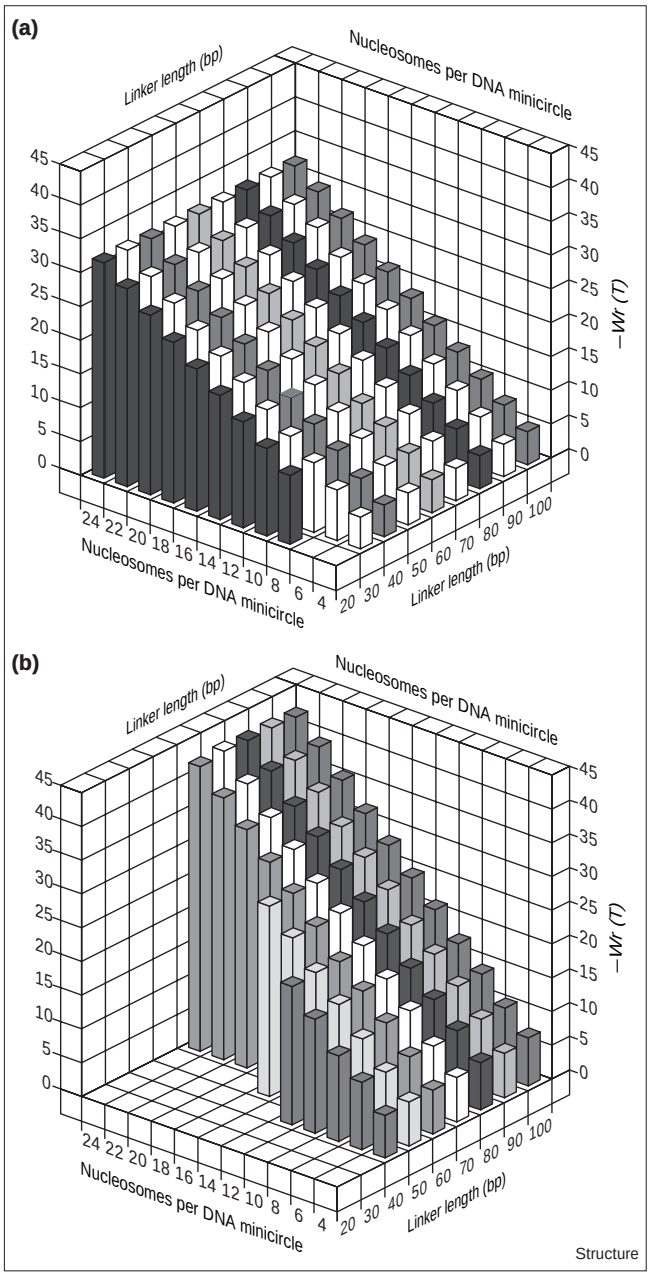

Three-dimensional plot of $-Wr$, the negative of the writhing number and a measure of global chain folding, as a function of linker length and number of nucleosomal constraints in minichromosome models confining (a) 1.5 and (b) 1.7 superhelical turns of DNA per protein core. The protein-bound DNA in these examples follows a regular superhelical path with R = 45 Å, P = 30 Å.

Table 2

Global equilibrium configurations of DNA rings bound by capstan-shaped nucleosomes on 207 bp repeat lengths.

R_e/R_0	T	N_{core}	Wr	R_e/R_0	T	N_{core}	Wr
1.46	1.5	4	–3.9	1.30	1.58	6	–5.0
		6	–6.0			8	–6.3
		8	–8.2			10	–7.9
		10	–10.0			12	–9.3
		22	–22.2			14	–10.7
1.44	1.51	4	–4.1	1.28	1.6	6	–5.2
		6	–6.2			8	–6.5
		8	–8.4			10	–7.9
		10	–10.5			12	–9.3
		14	–14.7			16	–12.5
		22	–23.2	1.26	1.61	6	–5.2
1.42	1.52	4	–4.2			8	–6.6
		6	–6.5			10	–7.9
		8	–8.7	1.24	1.62	8	–6.8
		10	–11.0			10	–7.8
		14	–15.5	1.22–1.16	1.63–1.66	–	–
		16	–17.7	1.14	1.67	4	–6.4
		20	–22.2			6	–10.0
1.40	1.53	4	–4.5			8	–13.7
		6	–7.0			10	–17.3
		8	–9.4			12	–21.0
		10	–11.9	1.12	1.68	4	–6.7
		12	–14.4			6	–10.1
		16	–19.3			8	–13.4
		18	–21.7			10	–18.2
		20	–24.1			14	–23.8
		24	–29.0	1.10	1.7	4	–6.5
1.38	1.54	4	–4.8			8	–13.9
		6	–7.6			10	–17.8
		8	–10.3			12	–21.8
		10	–13.2			14	–25.0
		12	–15.9	1.08	1.71	4	–6.5
		16	–21.3			6	–9.8
		18	–24.2			8	–14.2
		20	–26.9			10	–17.5
		24	–32.4			16	–28.5
1.36	1.55	4	–3.3	1.06	1.71	4	–6.2
		6	–4.4			6	–10.5
		8	–5.6			8	–14.3
		10	–6.7			12	–21.7
		12	–8.0			14	–25.0
		16	–10.4	1.04	1.73	4	–6.8
		18	–11.5			6	–10.3
		20	–12.7			8	–14.2
1.34	1.56	4	–3.4	1.02	1.74	4	–6.9
		6	–4.7			8	–14.3
		8	–5.9			12	–21.3
		10	–7.2	1.00	1.75	–	–
		14	–10.1				
		22	–15.1				
1.32	1.57	8	–6.2				
		10	–7.7				
		12	–8.8				
		14	–10.4				
		22	–15.9				

R_e/R_0 is the ratio of radii at the ends and center of the capstan-shaped nucleosomes, and T is the resulting number of turns of bound DNA. N_{core} is the number of core particles on the idealized DNA ring, and Wr is the writhing number, when R_0 = 45 Å. The variation of radius with turns t around the capstan is given by:

$$R(t) = R_0 \sqrt{1 + \left(\frac{t}{T}\right)^2 \left(\left(\frac{R_e}{R_0}\right)^2 - 1\right)}$$

for 1.5 superhelical turn complexes. The closed chains take up large numbers of such cores, which also confine ~1.5 turns of protein-bound DNA. In contrast, less deformed capstans, with $R_e/R_0 < 1.2$, wrapping more than 1.6 turns of DNA bind relatively few protein cores, again mimicking the behavior of chains with cylindrical nucleosomes. As expected from the folding of chains with cylinder-shaped octamers, the writhing numbers of chains with capstan cores increase with each addition of a nucleosome. The writhing number per nucleosome varies as much as 0.2 in chains with capstan cores of 47.7 Å outer radius ($R_e/R_0 = 1.06$), depending upon the number of bound nucleosomes (from –1.6 to –1.8 for $N_{core} = 4$–14). The minichromosomes binding capstan-shaped nucleosomes, however, do not foster the sharp changes in writhing number per nucleosome and do not register the monotonic decrease in *Wr* with uptake of superhelical wrapping seen in the cylinder-shaped cores. The data in Table 2 reveal a steady decrease in *Wr* per core, from approximately –1.0 to –1.3 as R_e/R_0 decreases from 1.46 to 1.38 and the number of superhelical turns concomitantly rises from 1.5 to 1.54. The values of nucleosomal *Wr*, however, jump to about –0.8 for core particles with 1.56–1.62 superhelical turns ($R_e/R_0 = 1.36$–1.24) and then drop back to values reminiscent of cylindrical cores (–1.7 to –1.8) for more than 1.67 turns ($R_e/R_0 < 1.14$). These large changes in writhing number hint at a dramatically different folding pattern for chains with capstan-style nucleosomes where $R_e = 1.24$–$1.36R_0$, compared to chains binding cores with greater or lesser deviations from a cylinder. Also notice that the capstan shapes that do not define any closed chains, where $R_e/R_0 = 1.16$–1.22 and 1.37, precisely flank the range of radial deformations that define the minichromosomes of lowest *Wr* per core. The closed chains apparently seek a new folding pattern when geometric reasons prohibit the formation of a given configurational motif. The missing chains suggest a folding transition.

To confirm this idea, depictions of representative structures with bound protein octamers of similar shape, but with decidedly different *Wr* per core values, are illustrated in Figure 4. Each of the chains binds 20 nucleosomes, one with $R_e = 1.36R_0$ and the others with $R_e = 1.38R_0$ and $1.42R_0$. The folding of the chain with intermediate R_e and 1.54 turns of bound DNA per core in Figure 4b is reminiscent of the 'refrigerator-coil' motif exhibited by minichromosomes wrapping 1.5 superhelical turns of DNA around cylindrical cores. This pattern, however, completely changes when the capstan is very slightly perturbed. The (1.54 to 1.55) increase in superhelical turns brought about by a small decrease in the outer radius of the capstan (from 62.1 Å when $R_e = 1.38R_0$ to 60.3 Å when $R_e = 1.36R_0$) reorients sequential nucleosomes and drastically collapses the minichromosome structure (see Figure 4a). The faces of successive nucleosomes run approximately perpendicular to each other in the latter minichromosome, whereas they adopt a roughly parallel arrangement in Figure 4b.

We have attempted to pinpoint the topological difference between the preceding two folding motifs by examining enlarged views of the global equilibrium configurations of chains with four capstan-shaped protein cores binding 1.55 and 1.54 turns of DNA. The 1.54-turn cores in Figure 5b introduce a crossing between linker segments that makes a negative contribution to the writhing number, whereas the 1.55-turn nucleosomes in Figure 5a adopt a reverse ring fold. This switches the sense of each inter-linker crossing, and thus the signs of their contributions to the writhing number [48]. Reversing the fold of an entire chromatin domain switches the sense and sign of every linker segment crossing and accounts for the large difference in *Wr* between chains binding such similarly shaped cores. This drop in the writhing number per nucleosome may be of biological relevance in that it reconciles experimental and theoretical understanding of nucleosome-driven chain folding. A low *Wr* per core motif is also encountered in models with DNA linkers under 60 bp and bound segments wrapping 1.55 or 1.6 superhelical turns around cylinder-shaped protein cores [49] (data not shown). Thus, the correspondence of computation with observed linking-number changes in minichromosomes (discussed below) does not necessarily require capstan-shaped deformations of the nucleosome.

A similar transformation of possibly equivalent genetic significance is encountered for capstan-shaped cores wrapping less than 1.54 superhelical turns of DNA. The decrease in superhelical wrapping brought about by a small increase in the outer radius of the capstan dramatically expands the global structure of the minichromosome. For example, a 3% change in protein shape (from $1.38R_0$ to $1.42R_0$) decreases DNA wrapping from 1.54 to 1.52 turns and nearly doubles the diameter of the closed multiprotein-bound DNA ring (from 544 to 969 Å, these values corresponding to twice the distance from the centers of the respective minichromosome models to the points where linker DNA exits each nucleosome). Consecutive nucleosomes shift from a nearly parallel alignment of 1.54-turn cores to a perpendicular arrangement of 1.52-turn cores; compare Figures 4b and 4c. Such an event, in which a small change in nucleosome shape drastically alters the structure of a minichromosome, provides a hypothetical mechanism of how acetylation or other core histone modifications might trigger the unfolding of a tightly packed, inactive chromatin domain for transcription. In summary, non-cylindrical protein constraints underscore a diversity of folding patterns in chromatin chains, and support sharp folding transitions with small variations in core dimensions. Future investigations of other distortions of the histone core, for example centrally budged, cut-off ellipsoidal shapes [33,45], may prove equally telling.

Figure 4

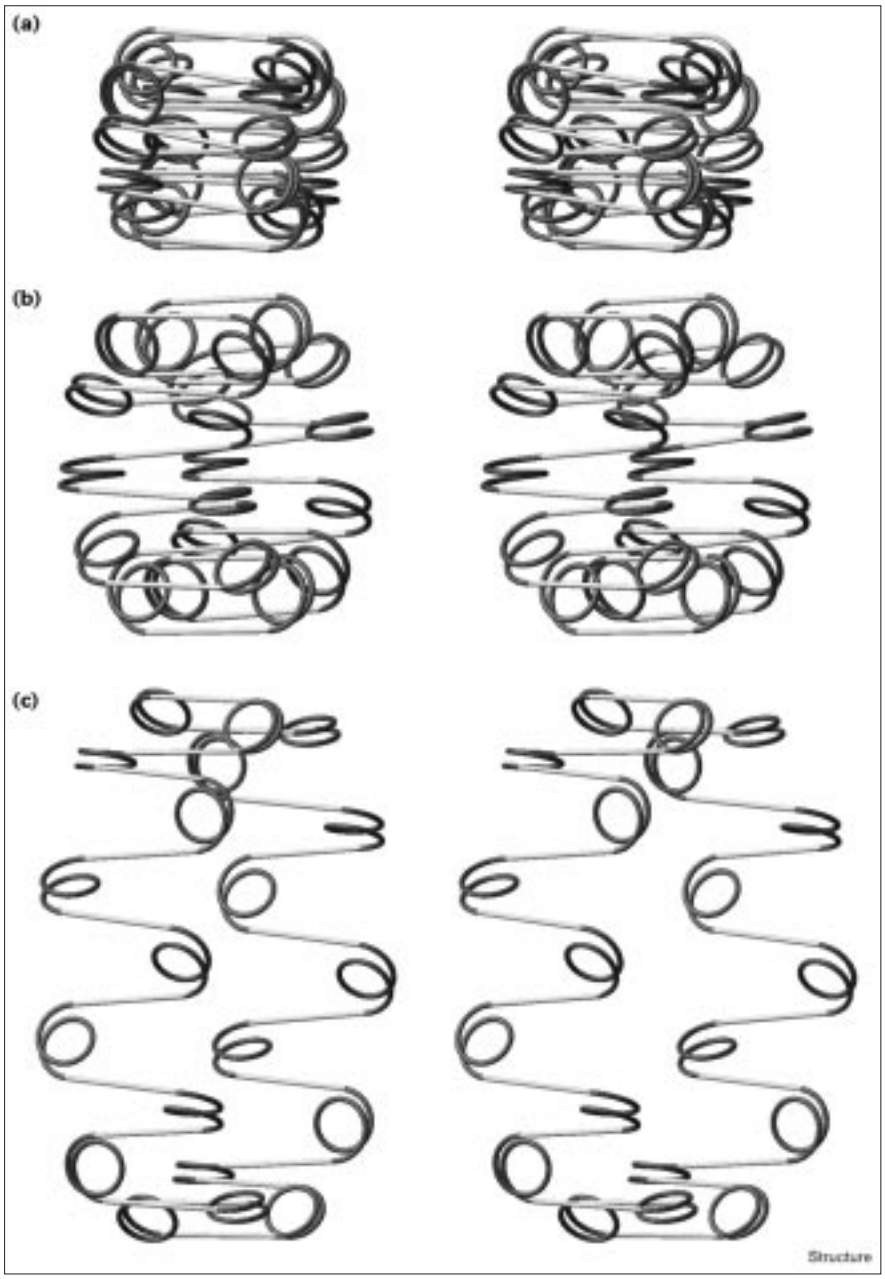

Stereoviews of global equilibrium structures of three minichromosome models, each binding 20 capstan-shaped, phantom histone octamers, illustrating the large configurational changes brought about by small deformations of protein shape. Nucleosomes with end-to-center radii ratios (R_e/R_0) of (a) 1.36, (b) 1.38, and (c) 1.42 constrain 146 bp of DNA to 1.55, 1.54, and 1.52 superhelical turns, respectively. Linker DNA is set at 61 bp in all cases.

Discussion

Real versus idealized minichromosomes

A number of significant properties of chromatin behavior and function have been revealed through the manipulation of minichromosomes. Although these imitation chromosomes have been employed freely in a wide variety of investigations, relatively few studies include actual views of the structures themselves [11–13,32]. Since even the most refined visualization techniques cannot yet resolve precise protein shapes or the path of DNA in a protein–nucleic acid complex, these parameters must be deduced through comparisons of computed structures with relevant experimental observations. Here we consider several electron microscopy (EM) studies of DNA minichromosomes in the context of our data.

Griffith's pioneering electron micrographs of native SV40 DNA [12] illustrate the compaction of the circular molecule from naked to histone-bound states well. Our models provide a variety of folding motifs, the majority of which condense closed circular DNA far beyond the five-fold reduction in length attributed to spooling the double

Figure 5

Enlarged stereoviews of the global equilibrium configurations of two minichromosome models binding four capstan-shaped phantom histone octamers apiece. Octamers with (a) R_e/R_0 = 1.36 and (b) R_e/R_0 = 1.38 constrain 146 bp of DNA to 1.55 and 1.54 superhelical turns, respectively, and illustrate the subtle changes in chain crossings brought about by slight deformation of protein shape. Linker DNA is fixed at 61 bp in both cases.

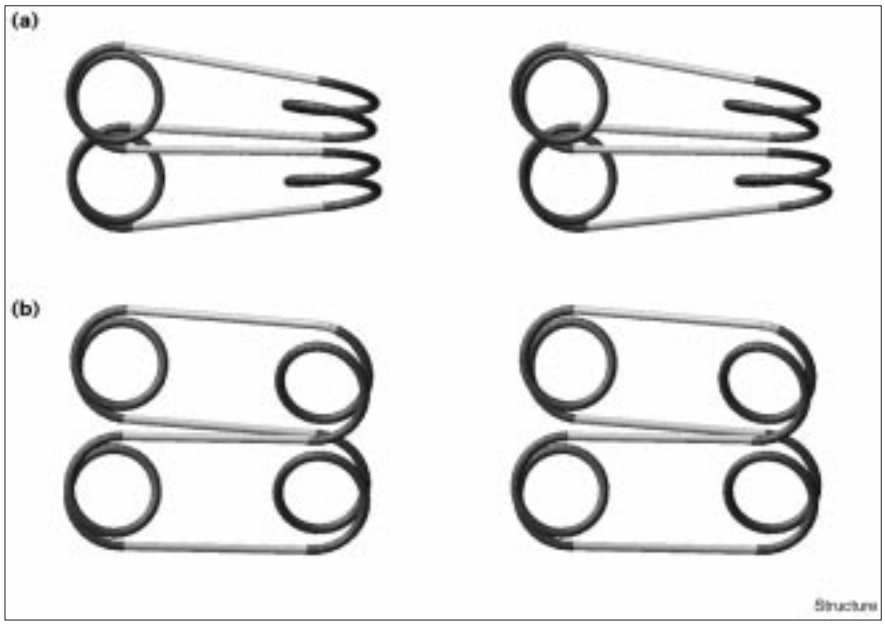

helix about a protein mass. The only exceptions are chains that constrain more than 1.85 superhelical turns of DNA per core particle. This elementary insight helps to hone in on a range of possible entry/exit angles for the DNA emerging from the nucleosome. Thus, the maximal wrapping around the core, consistent with the observed EM structures, precludes linker histone positioning that seals two full superhelical turns of DNA onto the octamer complex [50]. Instead, the linker histone may set a linear or more gradual superhelical track for the extra DNA that is bound in the chromatosome. Additional support for this idea is found in micrographs of minichromosomes reconstituted at a variety of histone and salt concentrations, with a range of acute, non-linear, entry/exit angles for the DNA emerging from the core [11,51]. Thus, our models help to distinguish between potentially artifactual data and valuable structural information related to the number of superhelical turns of bound DNA in real minichromosomes.

Information contained in our models also points to possible resolutions of the so-called linking-number paradox in minichromosomes. Gel analyses indicate that the amount of supercoiling introduced into SV40 by each histone octamer is approximately one negative supercoil per bound protein [11]. This value, though unexpectedly small on the basis of the number of superhelical turns of DNA observed in the nucleosome crystal structure [9], has found substantial support in minichromosome work, including complementary micrographs of a circular DNA with eighteen tandem repeats of a 207 bp nucleosome positioning sequence [13]. While the micrographs of these chains provide little information regarding higher order chromatin structures (i.e., chains appear as random, flattened coils), the accompanying sedimentation data [13] reveal a significant chain organization extending beyond the DNA in contact with protein, once two-thirds of the binding sites are complexed with histone aggregates. Figures 4a and 4b clearly demonstrate how this apparently disparate information can be synthesized harmoniously through the adoption of a chain fold previously proposed by Worcel and associates [19]. Constructs of minichromosomes binding either capstan-shaped nucleosomes with end-to-center radii ratios of 1.24–1.36 on 207 bp repeats or cylindrical cores constraining 1.55–1.6 superhelical turns of DNA between linker segments of 50 bp or less embody highly folded configurations of low writhing number. Specifically, the faces of successive nucleosomes on these chains are roughly perpendicular to one another, introducing 'positive' crossings between alternate nucleosomes and linkers that contribute to the observed writhing number (see Figure 5a). These 'long-range' interactions are quite different from the more localized positive crossings of linkers brought about by changes in the wrapping of DNA around individual nucleosomes [52].

Significant self-organization prevails among families of chains binding histones with less than 1.85 superhelical turns of DNA; for example, the 360 and 544 Å diameters of the cyclic DNAs binding 20 capstan-shaped cores in Figures 4a and 4b correspond respectively to 2.6% and 4.4% of the B-DNA contour. Moreover, these low *Wr* folding motifs (–0.6 and –1.3 per nucleosome, respectively) occupy cylindrical volumes roughly equivalent to the $\sim 2 \times 10^7$ Å^3 spherical space filled by the nucleohistone

core of the SV40 virus [53]. The sizes of the two assemblies, 3 and 7×10^4 Å^3, are estimated from the product of the ~300 Å height, that is, the sum of the linker length and nucleosome diameter, and the circular cross-sections, $\pi\rho^2$, where the global radii ρ are half the diameters noted above. The vacant cores of the models provide space for the proteins that must also pack inside the virus and suggest a mechanism potentially operative in the disassembly/assembly of the particle. Small changes in nucleosomal geometry can trigger an expansion of global structure, as in Figures 4b and 4c, which might disrupt the outer protein capsid.

Interpreting images of the 30 nm chromatin fiber

The wide array of torsionally relaxed minichromosome models derived here share traits in common with images of chromatin fibers provided by scanning-transmission EM [54], scanning-force microscopy [16,17,51], and electron tomography [15]. Simultaneously, they express different patterns in the folding of the nucleosome array. For example, the computed models place core particles at the periphery of the chromatin fiber, independent of linker length, core shape, amount of nucleosomal bound DNA, and number of protein constraints per chain, in agreement with many experimental views. Apparently, no matter how changes in salt or moisture level associated with different viewing practices might induce changes in the shapes, locations, or degrees of binding in the complexes, the cores should and do remain at the outer edges of the folded fiber, as both computational and experimental works report. Likewise, the short, linear, equal-length DNA linkers remain sequestered between flanking core particles in all views.

On the other hand, the orientations of linker segments and bound supercoils with respect to one another and the fiber axis differ substantially from one view, or model, to the next. Traditionally, the number of superhelical turns of DNA constrained by each nucleosome is expected to determine relative nucleosome and linker orientations [32,33]. The present chains bear out this finding. Nucleosome complexes wrapping 1.5 superhelical turns of DNA support face-to-face contacts between alternating nucleosomes [55], suggesting a solenoidal model for the fiber. In contrast, the smaller entry/exit angles for DNA issuing from 1.6- and 1.7-turn complexes (see Figures 2b and 2c) support edge-to-edge contacts between alternating bound supercoils, defining two-track, zig-zag models of DNA compaction. In brief, our models suggest that perhaps the diversity among observed fiber structures can be related back to small changes in the nucleosome repeat, which can, in turn, be attributed to mild variations in experimental conditions such as ionic concentration, level of genetic activity, and source of DNA.

The complexity of chromatin folding, however, continues with the recent publication of three-dimensional, low temperature *in situ* electron tomographs of radially arrayed, perpendicular nucleosomes [15]. Previously, only non-uniform linker lengths could account for this twisted zig-zag ribbon [16]. Importantly, the structures encountered here with a fixed linker length of ~50 bp (comparable to the average yielded by experiment) and variable local twist (brought about by flexible nucleosome-linker-nucleosome torsions), accurately mimic this new core arrangement (see Figure 6). Apparently, these circular chromatin fragments impose geometric constraints similar to those presented by higher order chromatin organization.

The present models also offer some hope in resolving an on-going controversy regarding fiber diameter–linker length correlations [56,57]. According to our data, alterations in the width of the two-nucleosome repeat, which sets the fiber diameter, are correlated directly with changes in the length of the spacer DNA. The rate of change in the fiber diameter also depends upon the entry/exit angle between the linker segments flanking the core. For instance, increases in linker length of octamers binding 1.5 superhelical turns of DNA are channeled directly into increasing the diameter of the fiber, since the linker segments run perpendicular to the fiber axis (see Figure 2a). If changes in ionic conditions or differences in H2A/H2B composition associated with different organisms or phases of the cell cycle diminish the electrostatic attraction between protein and DNA and induce the double helix to fray or peel away from the underlying protein surface and reduce the superhelical wrap to ~1.5 turn, the findings of Athey *et al.* [56] are well confirmed here. However, if the wrapping in the core is maintained in the cryogenically frozen sample as it is in the crystal structure, that is, 1.6–1.7 superhelical turns [9], a much smaller increase in the diameter of the 30 nm fiber would be registered by a large increase in linker length as reported by Woodcock [57]. It is apparent from Figures 2b and 2c that elongation of the spacer DNA would contribute as much to lengthening as widening the fiber. Our models thus offer a potential route to reconciliation of two conflicting views.

A different linking number problem

A well-documented yet lightly considered phenomenon associated with minichromosome topology is the less pronounced change in linking number observed when modified histones are reconstituted onto DNA rings. The complexation of hyperacetylated histones with circular DNA reduces the change in ΔLk per core (from roughly –1 in unmodified chains) to -0.81 ± 0.05 [58]. This is highly significant in that higher levels of histone acetylation in chromatin are directly tied to elevated transcriptional activity [59,60]. A popular explanation for the reduction in ΔLk is that acetylation alters the nucleosome in such a way as to release DNA from each protein mass and thereby

Figure 6

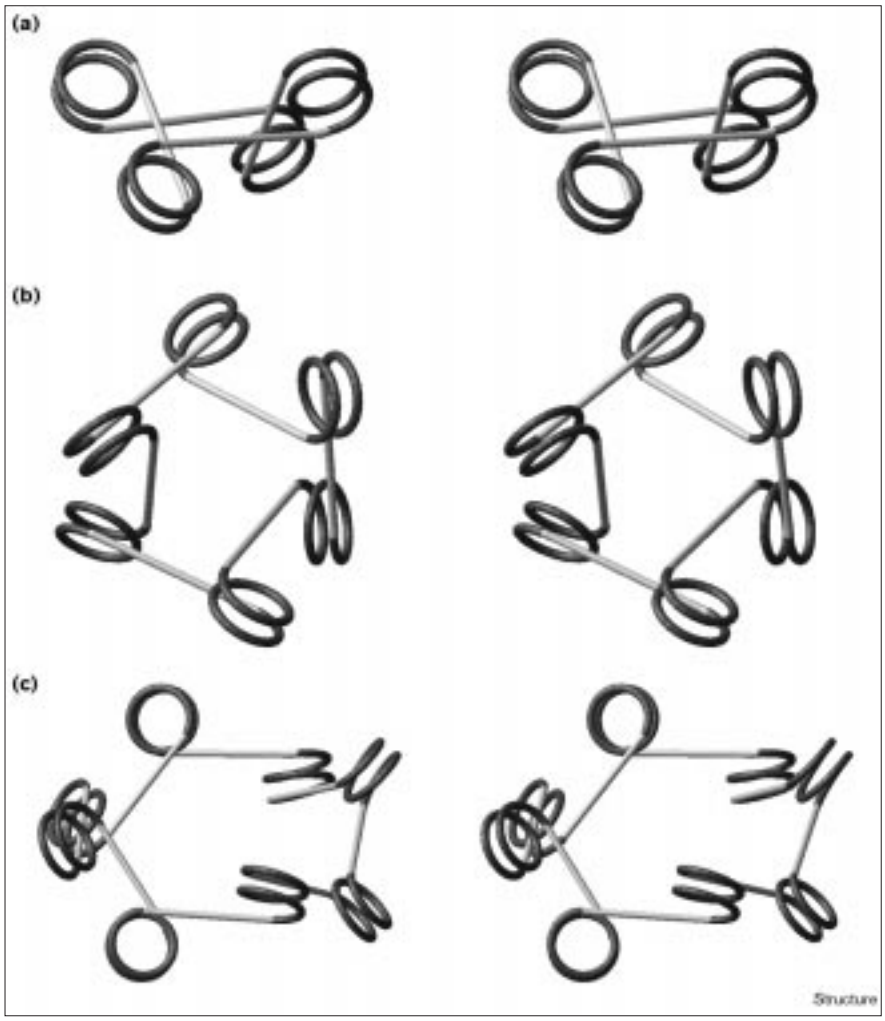

Stereoviews of the global equilibrium configurations of three minichromosomes binding (a) four, (b) six, and (c) eight cylindrical phantom histone octamers that mimic the twisted zig-zag chromatin ribbon [15]. Here, linker DNA is fixed at ~50 bp and protein-bound DNA spans ~1.7 superhelical turns.

diminish the amount of imposed supercoiling [27,28]; however, we find only a limited number of chains that bind traditional cylinder-shaped histone octamers and adopt a folding pattern where nucleosomal Wr is close to –1. (According to White's relationship between linking number, total twist, and writhing number, $\Delta Lk = \Delta Tw + Wr$ [61], ΔLk can be equated to Wr in torsionally relaxed chains where $\Delta Tw = 0$, as is assumed here.)

A simple alternative hypothesis, consistent with experimental measurements of ΔLk, can be derived from the data in Table 2. With 146 bp of DNA wound up to 1.62 superhelical turns around eight or more capstan-shaped protein solids, the writhing number per nucleosome never exceeds –0.9, and is as low as –0.6 in chains wrapping capstans with end-to-center radii ratios of 1.36. Such models are in excellent agreement with the ΔLk per core values determined experimentally and consistent with, but more pronounced than, the nucleosome distortions ($R_e/R_0 = 1.1$) proposed by Bauer and coworkers [30] from mathematical considerations of the octamer surface alone. Transcription-related modifications of the H3 and H4 histones that induce a change in the shape of the core particle instead of a loss of critical protein–DNA contacts could catalyze a switch in folding pattern throughout the entire genetic domain such as in Figures 4a and 4b with the net effect of reducing the writhing number per nucleosome. In brief, the coordinated change across a chromatin domain required for the onset of particular genetic processes may be driven by mild conformational alterations in the shapes of the packaging units themselves. Thus, our models not only address unified configurational shifts, but also account for experimentally deduced topological changes.

Biological implications

The nucleosome, the fundamental packaging unit of eukaryotic chromatin, shapes DNA at both the atomic and macromolecular levels. The global organization of

nucleosomes ensures the compaction necessary for packaging DNA inside the nucleus and provides the framework for genetic regulation. The tight wrapping of DNA about the core of eight histone proteins compacts the double helix significantly along a left-handed superhelical pathway [9]. The present computational examples illustrate the next level of chromatin organization, radial chromosome loops [10], as modeled in multinucleosomal DNA rings, or minichromosomes [11–13] that approximate biologically relevant structures.

The three-dimensional structures reported here, with up to 24 bound proteins, far exceed any previous minichromosome models [32–36] in both size and scope. The models not only mimic the size and nucleosome composition of the naturally occurring SV40 minichromosome [11,12] but also match the known nucleohistone volume of the virus [53]. The computed structures account as well for discrepancies among published images of the 30 nm chromatin fiber; for example, chains with nucleosomes wrapping 1.5 superhelical turns of DNA support the face-to-face contacts between alternating nucleosomes expected of a solenoidal fiber [18]. In contrast, the smaller entry/exit angles of the DNA issuing from 1.6- and 1.7-turn complexes support the edge-to-edge contacts between alternating bound supercoils anticipated in zig-zag models of DNA compaction [15,16]. In other words, the computed three-dimensional models suggest that the diversity among observed fiber structures may reflect small changes in DNA wrapping or nucleosomal shape, which may simply reflect minor variations in experimental conditions.

The structures further demonstrate the 'paradoxical' low-writhe folding patterns long anticipated from the electrophoretic behavior of minichromosomes [11,13]. The uptake in supercoiling associated with the assembly of nucleosomes on circular DNA (approximately one negative supercoil per bound protein core) is significantly lower than that (1.6–1.7 such supercoils) expected from the tertiary folding of DNA around the nucleosome core particle [32–36]. Here, we see that this well-known paradox [45,62] can be reconciled by a compact global folding motif that brings spatially distant linker segments into close contact along the lines originally suggested by Worcel and coworkers [19].

Finally, the present computer models illustrate potential mechanisms for chromatin reorganization through small, concerted changes in DNA wrapping or protein shape. Transcription-related modifications, in which a small change in nucleosome shape drastically alters the structure of a minichromosome, show how acetylation or other core histone modifications might trigger the unfolding of a tightly packed, inactive chromatin domain for transcription. Such conformational switches could facilitate the binding of the chromatin remodeling proteins that are required for transcription initiation [63]. Other conformational events that cause the release or uptake of a few base pairs of DNA on the nucleosome could similarly switch the global folding of a genetic domain and induce biological activity. By contrast, changes in linker length and number of bound proteins have a limited influence on the global folding simulated here and may not play as important a role in biochemical control.

Materials and methods

Representation of nucleosomal DNA

We generate idealized minichromosome models from linear segments of linker and nucleosomal elements. The linkers are modeled by vectors $\mathbf{v}_l$ equal in magnitude to the helical contour length of the protein-free double helical segments, and the nucleosomes by vectors $\mathbf{v}_n$ joining the ends of the superhelical-wrapped, protein-bound DNA (see Figure 1a). The linkers are assumed to be collinear with the tangential exit of DNA from the nucleosomes, so that the valence angles between nucleosome and linker, $\phi_{l-n} = \phi_{n-l}$, and the linker–nucleosome–linker torsion, τ_{l-n-l}, and the magnitude of $\mathbf{v}_n$ depend on the degree of superhelical wrapping and the assumed radius and pitch of the protein cores.

Construction of closed chains

The construction of closed chains with alternating linkers and nucleosomes entails the search of internucleosomal linker torsions, τ_{n-l-n}, that yield regular structures of zero pitch. The values of τ_{n-l-n} specify the twist of an un-nicked linker as well as the folding of adjacent nucleosomes, so that the imposed twist of an un-nicked chain is also a function of the assumed degree of wrapping and the proportions of the nucleosome. Here, we consider chains constructed from combinations of m successive τ_{n-l-n} values, the backbone conformation thus repeating every m nucleosomes. We make use of equations that relate backbone bonds and angles to the helical parameters of a regularly repeating chain molecule [64] in combination with a higher order virtual bond representation of the DNA–protein assembly. The virtual bond vector V is the resultant of the m nucleosomal and linker segments comprising the assumed conformational unit, that is,

$$\mathbf{V} = \sum_{i=1}^{m} (\mathbf{v}_{n_i} + \mathbf{v}_{l_i})$$

see Figure 1b where $m = 2$.

We obtain a set of 'backbone' parameters – a virtual 'bond length' V, a virtual 'valence' angle ϕ_V, and a virtual 'torsion' τ_V – by transforming the repeating nucleosome and linker segments into a common coordinate frame. The bond length V is obtained from the magnitude of V, the supplement of the bending angle ϕ_V from the scalar product of neighboring virtual bond vectors, and the torsion τ_V from the spatial disposition of three successive virtual bonds.

Helical parameters

The simplified (monomeric) chain backbone representation is easily converted with standard equations [64] into a helical framework (corresponding to the folding of nucleosomal superhelices and linkers into a regular quaternary structure). The helical repeating angle, θ, depends on the virtual bending ϕ_V and torsion τ_V angles,

$$\cos\left(\frac{\theta}{2}\right) = \cos\left(\frac{\tau_V}{2}\right)\sin\left(\frac{\phi_V}{2}\right) \quad (1)$$

while the helical displacement of conformational units, d, also reflects the repeating length V,

$$d \sin\left(\frac{\theta}{2}\right) = V \sin\left(\frac{\tau_V}{2}\right) \sin\left(\frac{\phi_V}{2}\right) \quad (2)$$

The number of bound nucleosomes per turn of helix, N_{core}, is obtained from θ and *m*, the assumed number of nucleosomes and linkers in the repeating conformational fragment, that is,

$$N_{core} = \left(\frac{2m\pi}{\theta}\right)$$

The global radius of the fourth-order helix, ρ, is a function of θ, *d*, and *V*,

$$\rho^2 = \frac{1}{2}\left(\frac{V^2 - d^2}{1 - \cos\theta}\right) \quad (3)$$

Perfect closed circular structures correspond to integral values of N_{core} and zero *d*. To screen out knotted structures, which are frequently encountered in condensed rings [49], we set a lower limit on *ρ* (see below).

Construction of model minichromosomes

For each virtual bond representation with acceptable helical parameters, the corresponding three-dimensional closed structure of alternating linker and nucleosome fragments is assembled. The molecular pieces are arranged so that their end-to-end vectors (v_n and v_l) describe the nucleosome–linker valence angles (ϕ_{l-n}, ϕ_{n-l}) and torsions (τ_{l-n-l}, τ_{n-l-n}) that lead to the desired global helical parameters: N_{core} = integer ± 0.05; *d* = 0 ± 0.05 Å; ρ > 100 Å. The limitations on N_{core} and *d* assure the formation of nearly perfect circular structures, while the limit on ρ reduces the likelihood of knot formation.

The allowed variation in helical parameters yields sets of similar chains with the same numbers and kinds of protein constraints. We limit our presentation to the configurations, within each pool of like minichromosomes, with the smallest gaps between chain ends. We further eliminate all structures with long-range steric clashes, arbitrarily choosing a 15 Å minimum contact limit between contour points on remote parts of the double helical axis. This contact limit, although smaller than the diameter of naked B-DNA, is consistent with the narrowing of the double helix brought about by limited stretching deformations [65]. Finally, we determine the writhing numbers, *Wr*, of the closed curves with a formulation developed by Irwin Tobias and defined elsewhere [36].

Although the examples presented here are limited to the study of DNAs with an even number of nucleosomes, the approach can be used to search for rings binding odd numbers of nucleosomes by accepting half integral values for the chain repeat. Thus, any minichromosome composed of tandem repeats of nucleosome positioning sequences or, indeed, any circular DNA containing assemblies of other DNA bending or wrapping proteins is within reach. The distortions of global chromatin structure brought about by thermal fluctuations of the DNA linkers and irregularities of nucleosomal wrapping are ignored in this treatment.

Acknowledgements

This work was taken in part from the dissertation of Jennifer A Martino written in partial fulfilment of the requirements for the degree of Doctor of Philosophy, Rutgers University, 1997. This research was generously supported by the US Public Health Service under research grant GM34809. JAM acknowledges a predoctoral fellowship from the Howard Hughes Medical Institute and VK postdoctoral support from the Program in Mathematics and Molecular Biology based at Florida State University. Calculations were performed at the Rutgers University Center for Computational Chemistry.

References

1. Hubbard, T.J.P., Murzin, A.G., Brenner, S.E. & Chothia, C. (1997). SCOP: a structural classification of proteins database. *Nucleic Acids Res.* 25, 236-239.
2. Wallace, A.C., Borkakoti, N. & Thornton, J.M. (1997). TESS: a geometric hashing algorithm for deriving 3D coordinate templates for searching structural databases. Application to enzyme active sites. *Protein Sci.* 6, 2308-2323.
3. Olson, W.K., Gorin, A.A., Lu, X.-J., Hock, L.M. & Zhurkin, V.B. (1998). DNA sequence-dependent deformability deduced from protein–DNA crystal complexes. *Proc. Natl Acad. Sci. USA* 95, 11163-11168.
4. Travers, A.A. (1989). DNA conformation and protein binding. *Annu. Rev. Biochem.* 58, 427-452.
5. Steitz, T.A. (1990). Structural studies of protein–nucleic acid interaction: the sources of sequence-specific binding. *Q. Rev. Biophys.* 23, 205-280.
6. Suzuki, M. & Yagi, N. (1995). Stereochemical basis of DNA bending by transcription factors. *Nucleic Acids Res.* 23, 2083-2091.
7. Pérez-Martin, J. & deLorenzo, V. (1997). Clues and consequences of DNA bending in transcription. *Annu. Rev. Microbiol.* 51, 593-628.
8. Schild, C., Claret, F.-X., Wahli, W. & Wolffe, A.P. (1993). A nucleosome-dependent static loop potentiates estrogen-regulated transcription from the *Xenopus* vitellogenin B1 promoter *in vitro*. *EMBO J.* 12, 423-433.
9. Luger, K., Mader, A.W., Richmond, R.K., Sargent, D.F. & Richmond, T.J. (1997). Crystal structure of the nucleosome core particle at 2.8 Å resolution. *Nature* 389, 251-260.
10. Marsden, M.P.F. & Laemmli, U.K. (1979). Metaphase chromosome structure: evidence for a radial loop model. *Cell* 17, 849-858.
11. Germond, J.E., Hirt, B., Oudet, P., Gross-Bellard, M. & Chambon, P. (1975). Folding of the DNA double helix in chromatin-like structures from simian virus 40. *Proc. Natl Acad. Sci. USA* 72, 1843-1847.
12. Griffith, J.D. (1975). Chromatin structure: deduced from a minichromosome. *Science* 187, 1202-1203.
13. Simpson, R.T., Thoma, F. & Brubaker, J.M. (1985). Chromatin reconstituted from tandemly repeated cloned DNA fragments and core histones: a model system for study of higher order structure. *Cell* 42, 799-808.
14. Woodcock, C.L., Grigoryev, S.A., Horowitz, R.A. & Whitaker, N. (1993). A chromatin folding model that incorporates linker variability generates fibers resembling native structures. *Proc. Natl. Acad. Sci. USA* 90, 9021-9025.
15. Horowitz, R.A., Agard, D.A., Sedat, J.W. & Woodcock, C.L. (1994). The three-dimensional architecture of chromatin *in situ*: electron tomography reveals fibers composed of a continuously variable zig-zag nucleosomal ribbon. *J. Cell. Biol.* 125, 1-10.
16. Leuba, S.H., Yang, G., Robert, C., Samori, B., van Holde, K., Zlatanova, J. & Bustamante, C. (1994). Three-dimensional structure of extended chromatin fibers as revealed by tapping mode scanning force microscopy. *Proc. Natl Acad. Sci. USA* 91, 11621-11625.
17. Yang, G., Leuba, S.H., Bustamante, C., Zlatanova, J. & van Holde, K. (1994). Role of linker histones in extended chromatin fibre structure. *Nat. Struct. Biol.* 1, 761-763.
18. Finch, J.T. & Klug, A. (1976). Solenoidal model for superstructure in chromatin. *Proc. Natl Acad. Sci. USA* 73, 1897-1901.
19. Worcel, A., Strogatz, S. & Riley, D. (1981). Structure of chromatin and the linking number of DNA. *Proc. Natl. Acad. Sci. USA* 78, 1461-1465.
20. Woodcock, C.L., Frado, L.L.Y. & Rattner, J.B. (1984). The higher order structure of chromatin. *J. Cell Biol.* 99, 42-52.
21. Williams, S.P., Athey, B.D., Muglia, L.J., Schappe, R.S., Gough, A.H. & Langmore, J.P. (1986). Chromatin fibers are left-handed double helices with diameter and mass per unit length that depend on linker length. *Biophys. J.* 49, 233-248.
22. Bishop, T.C., Kosztin, D. & Schulten, K. (1997). How hormone receptor–DNA binding affects nucleosomal DNA: the role of symmetry. *Biophys. J.* 72, 2056-2067.
23. van Holde, K.E. (1989). *Chromatin*. Springer-Verlag, New York.
24. Inaga, S., Osatake, H. & Tanak, K. (1991). SEM images of DNA double helix and nucleosomes observed by ultrahigh resolution scanning electron microscopy. *J. Electron Microsc.* 40, 181-186.
25. Fritzsche, W. & Henderson, E. (1996). Scanning force microscopy reveals ellipsoid shape of chicken erythrocyte nucleosomes. *Biophys J.* 71, 2222-2226.
26. Pruss, D., Bartholomew, B., Persinger, J., Hayes, J., Arents, G., Moudrianakis, N. & Wolffe, A.P. (1996). An asymmetric model for the nucleosome: a binding site for linker histones inside the DNA gyres. *Science* 274, 614-617.
27. Chen, T.A., Sterner, R., Cozzolino, A. & Allfrey, V.G. (1990). Reversible and irreversible changes in nucleosome structure along the c-fos and c-myc oncogenes following inhibition of transcription. *J. Mol. Biol.* 212, 481-493.

28. Oliva, R., Bazett-Jones, D.P., Locklear, L. & Dixon, G.H. (1990). Histone hyperacetylation can induce unfolding of the nucleosome core particle. *Nucleic Acids Res.* 18, 2739-2747.
29. Wolffe, A.P. & Dimitrov, S. (1993). Histone-modulated gene activity: developmental implications. *Crit. Revs. Eukaryotic Gene Expression* 3, 167-191.
30. Bauer, W.R., Hayes, J.J., White, J.H. & Wolffe, A.P. (1994). Structural changes due to acetylation. *J. Mol. Biol.* 236, 685-690.
31. Horowitz, R.A., Koster, A.J., Walz, J. & Woodcock, C.L. (1997). Automated electron microscope tomography of frozen-hydrated chromatin: the irregular three-dimensional zigzag architecture persists in compact, isolated fibers. *J. Struct. Biol.* 120, 353-362.
32. Zivanovic, Y., Goulet, I., Révet, B., Le Bret, M. & Prunell, A. (1988). Chromatin reconstitution on small DNA rings. II. DNA supercoiling on the nucleosome. *J. Mol. Biol.* 200, 267-290.
33. Zhang, P., Tobias, I. & Olson, W.K. (1994). Computer simulation of protein-induced structural changes in closed circular DNA. *J. Mol. Biol.* 242, 271-290.
34. Olson, W.K., Westcott, T.P., Martino, J.A. & Liu, G.-H. (1996). Computational studies of spatially constrained DNA. In *Mathematical Approaches to Biomolecular Structure and Dynamics.* (Mesirov, J.P., Schulten, K. & Sumners, D.W., eds), pp. 195-218, Springer-Verlag, New York.
35. Martino, J.A. & Olson, W.K. (1998). Modeling chain folding in protein-constrained circular DNA. *Biophys. J.* 74, 2491-2500.
36. Martino, J.A. & Olson, W.K. (1997). Modeling protein-induced configurational changes in DNA minicircles. *Biopolymers* 41, 419-430.
37. Compton, J.L., Bellard, M. & Chambon, P. (1976). Biochemical evidence of variability in the DNA repeat length in the chromatin of higher eukaryotes. *Proc. Natl Acad. Sci. USA* 73, 4382-4386.
38. Ulanovsky, L.E. & Trifonov, E.N. (1986). A different view point on the chromatin higher order structure: steric exclusion effects. In *Biomolecular Stereodynamics*, Vol. 3 (Sarma, R.H. & Sarma, M.H., eds), pp. 35-44, Adenine Press, Guilderland, NY.
39. Hagerman, P.J. (1988). Flexibility of DNA. *Annu. Rev. Biophys. Biophys. Chem.* 17, 265-286.
40. Langowski, J., Olson, W.K., Pedersen, S.C., Tobias, I., Westcott, T.P. & Yang, Y. (1996). DNA supercoiling, localized bending and thermal fluctuations. *Trends Biochem. Sci.* 21, 50.
41. Noll, M. (1974). Internal structure of the chromatin subunit. *Nucleic Acids Res.* 1, 1573-1578.
42. Lutter, L. (1978). Kinetic analysis of deoxyribonuclease I cleavage sites in the nucleosome core: evidence for a DNA superhelix. *J. Mol. Biol.* 124, 391-420.
43. Cockell, M., Rhodes, D. & Klug, A. (1983). Location of the primary sites of micrococcal nuclease cleavage on the nucleosome core. *J. Mol. Biol.* 170, 423-446.
44. Libertini, L.J. & Small, E.N. (1982). Effects of pH on low salt transition in chromatin core particles. *Biochemistry* 21, 3327-3334.
45. White, J.H., Gallo, R. & Bauer, W.R. (1989). Effect of nucleosome distortion on the linking deficiency in relaxed DNA minichromosomes. *J. Mol. Biol.* 207, 193-199.
46. Furrer, P., Bednar, J., Dubochet, J., Hamiche, A. & Prunell, A. (1995). DNA at the entry-exit of the nucleosome observed by cryoelectron microscopy. *J. Struct. Biol.* 114, 177-183.
47. Hamiche, A., Carot, V., Alilat, M., De Lucia, F., O'Donohue, M.-F., Révet, B. & Prunell, A. (1996). Interaction of the histone $(H3\text{-}H4)_2$ tetramer of the nucleosome with positively supercoiled DNA minicircles: potential flipping of the protein from a left to a right-handed superhelical form. *Proc. Natl Acad. Sci. USA* 93, 7588-7593.
48. Fuller, F.B. (1971). The writhing number of a space curve. *Proc. Natl Acad. Sci. USA* 68, 815-819.
49. Martino, J.A. (1997) "Modeling Global Equilibrium Configurations of Protein-constrained Circular DNA," Ph.D. Thesis, Rutgers, the State University of New Jersey, New Brunswick, NJ.
50. Boulikas, T., Wiseman, J.M. & Garrard, W.T. (1980). Points of contact between H1 and the histone octamer. *Proc. Natl Acad. Sci. USA* 77, 127-131.
51. Leuba, S.H., Bustamante, C., Zlatanova, J. & van Holde, K. (1998). Contributions of linker histones and histone H3 to chromatin structure: scanning force microscopy studies on trypsinized fibers. *Biophys. J.* 74, 2823-2829.
52. De Lucia, F., Alilat, M., Sivolob, A. & Prunell, A. (1999). Nucleosome dynamics. III. Histone tail-dependent fluctuation of nucleosomes between open and closed DNA conformations. Implications for chromatin dynamics and the linking number paradox. A relaxation study of mononucleosomes on DNA minicircles. *J Mol Biol.* 285, 1101-1119.
53. Baker, T.S., Drak, J. & Bina, M. (1988). Reconstruction of the three-dimensional structure of simian virus 40 and visualization of the chromatin core. *Proc. Natl Acad. Sci. USA* 85, 422-426.
54. Gerchman, S.E. & Ramakrishnan, V. (1987). Chromatin higher order structure studied by neutron scattering and scanning transmission electron microscopy. *Proc. Natl Acad. Sci. USA* 84, 7802-7806.
55. Lohr, D. & van Holde, K.E. (1979). Organization of spacer DNA in chromatin. *Proc. Natl Acad. Sci. USA* 76, 6325-6330.
56. Athey, B.D., Smith, M.F., Rankert, D.A., Williams, S.P. & Langmore, J.P. (1990). The diameters of frozen-hydrated chromatin fibers increase with DNA linker length: evidence in support of variable diameter models for chromatin. *J. Cell. Biol.* 111, 795-806.
57. Woodcock, C.L. (1994). Chromatin fibers observed *in situ* in frozen hydrated sections. Native fiber diameter is not correlated with nucleosome repeat length. *J. Cell Biol.* 125, 11-19.
58. Norton, V.G., Imai, B.S., Yau, P. & Bradbury, E.M. (1989). Histone acetylation reduces the nucleosome core particle linking number change. *Cell* 57, 449-457.
59. Gorovsky, M.A., Pleger, G.L., Keevert, J.B. & Johmann, C.A. (1973). Studies on histone fraction F2A1 in macro and micronuclei of *Tetrahymena pyriformis*. *J. Cell Biol.* 57, 773-781.
60. Hebbes, T.R., Thome, A.W. & Crane-Robinson, C. (1988). A direct link between core histone acetylation and transcriptionally active chromatin. *EMBO J.* 7, 1395-1402.
61. White, J.H. (1969). Self-linking and the Gauss integral in higher dimensions. *Am. J. Math.* 91, 693-728.
62. Klug, A. & Travers, A.A. (1989). The helical repeat of nucleosome-wrapped DNA. *Cell* 56, 10-11.
63. LeRoy, G., Orphanides, G., Lane, W.S. & Reinberg, D. (1998). Requirement of RSF and FACT for transcription of chromatin templates *in vitro*. *Science* 282, 1900-1904.
64. Miyazawa, T. (1961). Molecular vibrations and structure of high polymers. II. Helical parameters of infinite polymer chains as functions of bond lengths, bond angles, and internal rotation angles. *J. Polymer Sci.* 55, 215-231.
65. Kosikov, K.M., Gorin, A.A., Zhurkin, V.B. & Olson, W.K. (1999). DNA stretching and compression: large-scale simulations of double helical structures. *J. Mol. Biol.* 289, 1301-1326.